Theoretical analyses of space-charge doping in amorphous semiconductor superlattices. I. Doping superlattices

Inan Chen
Xerox Corporation, Webster Research Center, 800 Phillips Road, Webster, New York, 14580
(Received 1 October 1984)

A theoretical analysis of space-charge doping in "*n-i-p-i*" doping superlattices, in particular of amorphous semiconductors, is presented. It is shown that space-charge doping decreases the interlayer barrier height, and hence is a counterdoping. This accounts for the observed blue shift of photoluminescence. The decrease of barrier with the layer thickness also suggests the existence of an optimum thickness at which the quantum effect is most significant. In heavily doped hydrogenated amorphous silicon, this thickness is calculated to be several tens of nanometers. This result is consistent with the observation of persistent photoconductivity in superlattices of this layer thickness.

I. INTRODUCTION

There has been considerable interest in fabricating and characterizing superlattices which consist of alternating layers of amorphous semiconductors and/or insulators. This idea follows from the successful demonstrations of crystalline III-V compound superlattices.[1] In this case, the requirement of a close match in the crystal lattices between the two layer materials limits the range of materials from which superlattices can be fabricated. With amorphous materials, since the lattice itself is disordered, it is hoped that the above requirement may be relaxed and superlattices can be formed with a wider variety of materials, and in large areas. In fact, superlattices made from tetrahedrally bonded amorphous materials, e.g., hydrogenated silicon, carbon, silicon nitrides, and silicon oxides, have been reported in the literature.[2–7] This new type of materials exhibits electronic properties which are of great scientific interest and may have practical applications.

An important phenomenon in superlattices is the space-charge doping that arises from charge transfer through the interfaces. This causes the band edges near the interfaces to bend upward or downward depending on the sign of charge transferred. If the thickness of each individual layer (referred to as "layer thickness" hereafter) is larger than or equal to the depletion width, the band edges at the center of the layer relax to their bulk positions. However, as the layer thickness is reduced, the layer becomes fully depleted and the band edges are not located at their bulk positions even in the middle of the layer. This can change the effective value of the barrier height. In general, if electrons are injected into an electron well (i.e., a well in the conduction band), or holes into a hole well (i.e., a well in the valence band), the barrier height increases. On the other hand, if electrons are injected into a hole well, or holes into an electron well, then the barrier height is decreased. In "*n-i-p-i*" doping superlattices,[1] as shown in Fig. 1, the electron well is in the *n*-type layers and the hole well is in the *p*-type layers. The charge carriers injected are always the minority carriers. The actual band edges are deformed as shown by the dashed curves in Fig. 1. The space-charge doping reduces the barrier heights (indicated by Δ in Fig. 1) at both the conduction and the valence bands from the value determined from the difference between the Fermi energies of the two layers (Δ_0). The thinner the layer is, the smaller the barrier becomes. For the quantum effect to be significant, a small layer thickness and a large barrier height is required. Therefore, the existence of an optimum thickness for maximum quantum effect in doping superlattices is expected.

In this paper, we present a theoretical analysis of the space-charge-doping process in doping superlattices. This involves the calculations of (1) the electronic potential distributions in the multilayer, and (2) the quantized energy and the wave function of an electron in this potential. The mathematical procedures are described in Sec. II. Although the general formulas are applicable to amorphous as well as crystalline semiconductor superlattices, numerical results are generated for superlattices made from hydrogenated amorphous silicon (*a*-Si:H). These results are presented and discussed in Sec. III. A similar analysis for compositional superlattices are reported in the accompanying paper.[8]

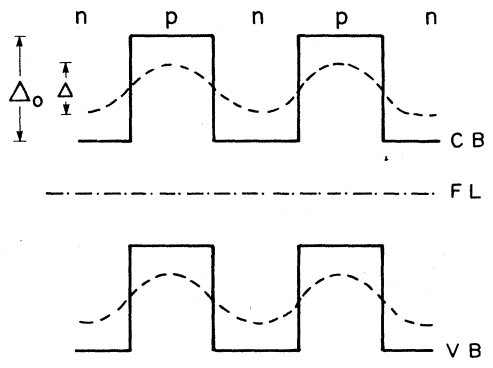

FIG. 1. The conduction band (CB), the valence band (VB), and the Fermi level (FL) in an *n-p* doping superlattice. The solid lines represent the nominal position while the dashed curves show the actual positions of the band edge due to space-charge doping. The barrier height Δ is reduced from the nominal value Δ_0.

II. MATHEMATICAL PROCEDURES

A. Electronic potential distributions

Poisson's equation for the electronic potential energy V (in units of k_BT) is,

$$d^2V/dx^2=(q/\epsilon k_BT)[q(p-p_0-n+n_0)+Q_L] , \quad (1)$$

where q is the elemental charge, ϵ is the permittivity, k_B is the Boltzmann constant, and T is the absolute temperature. The space-charge density on the right-hand side of Eq. (1) consists of two parts. The first part represents the charge of the excess free carriers due to band bending. By using this quantity instead of the charge of ionized dopants, the resultant potential is self-consistent. The hole and the electron densities, p and n, respectively, and their equilibrium (bulk) values, p_0 and n_0, can be expressed in terms of the intrinsic carrier density n_i, the (bulk) Fermi energy E_F^0, the hole quasi-Fermi-energy E_F^h, and the electron quasi-Fermi-energy E_F^e, with

$$p=n_i\exp(V-E_F^h) ; \quad p_0=n_i\exp(-E_F^0) , \quad (2)$$

$$n=n_i\exp(E_F^e-V) ; \quad n_0=n_i\exp(E_F^0) , \quad (3)$$

where the energies are measured in units of k_BT from the midgap.

The second component of the space charge Q_L, unique to amorphous materials, arises from the excess charge in the localized gap states. The typical distributions of donorlike gap states $N_{DL}(E)$ and the acceptorlike gap states $N_{AL}(E)$ can be approximated by the exponential functions (see Fig. 2),

$$N_{DL}(E)=N_L\exp(-E/w) , \quad (4)$$

$$N_{AL}(E)=N_L\exp(E/w) , \quad (5)$$

where the energy E is also measured in units of k_BT from the midgap. The parameters N_L and w are not necessarily the same for the two distributions. The former represents the density at the midgap, and the latter characterizes the exponential increase of the distribution as E approaches the band edges. A donorlike state is neutral when occupied and positively charged when empty (i.e., when it lies above the Fermi level). An acceptorlike state is neutral when empty and negatively charged when occupied (i.e., when it lies below the Fermi level). Thus, the space charge in the localized states due to a shift in the Fermi level Q_L is schematically illustrated in Figs. 2(b) and 2(c). Using the above two idealized distributions and the "zero temperature" statistics, one obtains[9–11]

$$Q_L(V)=qk_BTwN_L\{\exp[(V-E_F^h)/w]-\exp[(E_F^e-V)/w] +2\sinh(E_F^0/w)\} . \quad (6)$$

When the multilayer is in equilibrium the quasi-Fermi-levels are constant across the layers and can be set as $E_F^h=E_F^e=0$. The Debye lengths with respect to the intrinsic carrier density D_i and that with respect to the localized state density D_L can be defined by

$$D_i=(\epsilon k_BT/q^2n_i)^{1/2} , \quad (7)$$

$$D_L=(\epsilon/q^2N_L)^{1/2} . \quad (8)$$

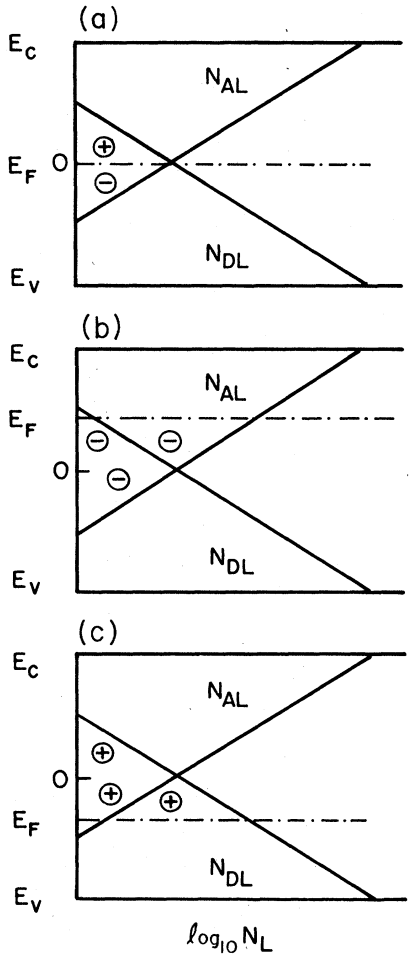

FIG. 2. Model of localized state distributions in the band gap of amorphous semiconductors: (a) for intrinsic material with the Fermi level E_F at the midgap; (b) with the Fermi level in the upper half-gap $E_F>0$; and (c) with the Fermi level at lower half-gap.

Using the Debye lengths and Eqs. (2), (3), and (6), Eq. (1) can be rewritten for the equilibrium condition as

$$d^2V/dx^2=2[\sinh(V)+\sinh(E_F^0)]/D_i^2 +2w[\sinh(V/w)+\sinh(E_F^0/w)]/D_L^2 . \quad (9)$$

This equation is to be solved numerically by the relaxation method over a period ($-S\le x\le S$), consisting of p-, i-, and n-type layers, shown in Fig. 3. However, because of the mirror symmetry of V with respect to the midplane of each layer, it is necessary to solve only within a half period from $x=-S/2$ to $S/2$. The boundary conditions at these points are

$$dV/dx=0 \quad \text{at } x=-S/2 \text{ and } S/2 . \quad (10)$$

Furthermore, if the p- and n-type materials are antisymmetric with respect to the zero of energy (i.e., the midgap) i.e., their Fermi energies are related by $E_F^p=-E_F^n$ and the layers are of the same thickness, then only the solutions in a quarter period from $x=0$ to $x=S/2$ are necessary. In this case, the boundary condition at $x=0$ is $V(0)=0$ (for

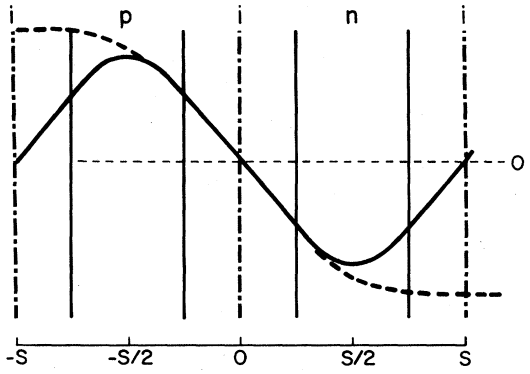

FIG. 3. Schematic of a potential distribution in an n-i-p-i superlattice, and the coordinate system used in the text.

the i-type layer $E_F^0=0$).

The potential distributions obtained above can be used to calculate the electronic sheet conductance G from the expression,

$$G=q\mu\int_0^{S/2} n(x)dx=q\mu n_i\int_0^{S/2}\exp[-V(x)]dx\ , \tag{11}$$

where μ is the electron mobility.

B. Quantized energies and wave functions

The wave function for an electron in a one-dimensional periodic potential can be written as a modulated plane wave,

$$\psi=U(k,x)\exp(ikx)\ , \tag{12}$$

where k is the wave vector and $U(k,x)$ is a periodic function with a period $2S$. With this wave function, the one-dimensional Schrödinger equation reads[12]

$$d^2U/dx^2+2ik(dU/dx)+(2m^*/\hbar^2)[E-E_k-V(x)]U=0 \tag{13}$$

where $E_k=(\hbar k)^2/2m^*$, m^* is the electron effective mass, and $V(x)$ is the periodic potential. For a square-well potential, the solutions of Eq. (13) can be expressed in terms of analytic functions,[12] and the energy levels E and wave functions can be obtained by numerical solutions of a transcendental equation. For a periodic potential of general shape, such as those obtained numerically in the previous subsection, the quantized energy level E and the wave function U must be obtained from direct numerical integration of the differential equation, Eq. (13). The procedure is described below.

First, the lowest-order quantized energy E can be determined by integrating Eq. (13) over a period, $x=0$ to $x=2S$. Using the periodic boundary conditions: $U(k,0)=U(k,2S)$ and $[dU/dx]_{x=0}=[dU/dx]_{x=2S}$, one obtains

$$E=E_k+\frac{\int_0^{2S}V(x)U(k,x)dx}{\int_0^{2S}U(k,x)dx}\ . \tag{14}$$

Denoting the real and the imaginary parts of U as u and w, respectively, and substituting into Eq. (13), one gets the following two equations:

$$d^2u/dx^2-2k\,dw/dx+(2m^*/\hbar^2)[E-E_k-V(x)]u=0\ , \tag{15}$$

$$d^2w/dx^2+2k\,du/dx+(2m^*/\hbar^2)[E-E_k-V(x)]w=0\ . \tag{16}$$

Similarly, Eq. (14) can be rewritten as

$$E=E_k+\frac{\left[\int Vu\,dx\right]\left[\int u\,dx\right]+\left[\int Vw\,dx\right]\left[\int w\,dx\right]}{\left[\int u\,dx\right]^2+\left[\int w\,dx\right]^2}\ , \tag{17}$$

with

$$\left[\int Vw\,dx\right]\left[\int u\,dx\right]-\left[\int Vu\,dx\right]\left[\int w\,dx\right]=0\ , \tag{18}$$

where all integrals are taken over a period $0\le x\le 2S$. The three quantities u, w, and E can be solved from Eqs. (15)—(17) by the relaxation method until self-consistency, using Eq. (18) as a supplemental criterion.

III. RESULTS AND DISCUSSION

A. Electronic potential distributions

Figure 4 shows examples of calculated potential distributions in the quarter period $x=0$ to $S/2$ (see Fig. 3) for an antisymmetric p-n multilayer (no i layers), with $E_F^0=24(k_BT)$. The potential distribution in the p layer

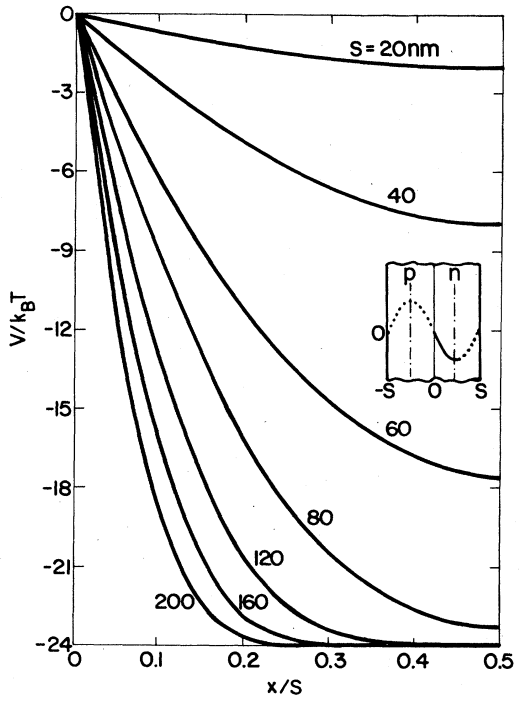

FIG. 4. Calculated potential distribution in a quarter period (solid-line portion in the inset) for an antisymmetric n-p multilayer of Fermi energies $E_F=\pm 24k_BT$ and various thicknesses S. The Debye lengths are $D_i=10^6$ nm and $D_L=10^3$ nm.

and the other half of the n layer can be generated by mirror images of this curve as illustrated in the inset. The layer thickness S is varied from 20 to 200 nm. The Debye lengths are $D_i = 10^6$ nm and $D_L = 10^3$ nm. The former corresponds to an intrinsic carrier density of $n_i = 1.65 \times 10^7$ cm^{-3} which is consistent with the dark resistivity of undoped a-Si:H (with Fermi level $E_F = 6$) being $\approx 10^9$ Ω cm.[13] The D_L value corresponds to the midgap density of $N_L = 0.66 \times 10^{15}$ cm^{-3} eV^{-1}. The parameter $w = 2.85$ is chosen so that the exponential distributions of localized states increase to a value of 10^{20} cm^{-3} eV^{-1} at the band edges ($E = \pm 34 k_B T$).

The barrier height which is the difference between the potential at the center of the p-type layer and that at the center of the n-type layer, is equal to twice the absolute value of V at $x = S/2$. It can be seen from Fig. 4 that as a result of space-charge doping, the barrier height decreases significantly with the layer thickness. Figure 5 shows the barrier height as a function of the layer thickness, calculated for various doping levels of the p- and n-type layer, represented by the Fermi energy E_F^0. For the solid curves, the density of intrinsic carriers and the localized state distribution are the same as those used in Fig. 4. One can see that the barrier height can maintain the value determined by the difference of the Fermi energies ($2E_F^0$ in this case) to a smaller thickness only if the doping level is higher. However, even at $E_F^0 = 24 k_B T$, which at room temperature ($k_B T \approx 0.025$ eV) is almost the upper limit for a-Si:H,[13] the barrier height is reduced to less than half at thicknesses less than 50 nm. This conclusion is also valid for other localized state densities (or D_L), as shown by the dashed curves in Fig. 5. The curve with $D_L = \infty$ represents a multilayer in which the localized-state density is negligibly small (e.g., crystalline).

From the reduction of barrier height shown above, it can be said that space-charge doping in n-p superlattices is in fact equivalent to a counter doping. The doped semiconductor layers behave electronically more intrinsic. Since the photoluminescence peaks are found[14] to shift toward longer wavelengths as the doping level in a-Si:H is increased, one can expect the photoluminescence of n-p superlattices to peak at a shorter wavelength than that of the unlayered constituent a-Si:H. This is indeed observed experimentally.[7]

Assuming the mobility to be independent of the layer thickness, one obtains the sheet conductance G, Eq. (11), as a function of the layer thickness S as shown in Fig. 6. The conductance is normalized to the "intrinsic" sheet conductance $G_i = q\mu n_i S/2$. In the limit of infinitely thick layers, the normalized sheet conductance approaches $\exp(E_F^0)$. The values of D_i and D_L are the same as those used in Fig. 5 for the solid and dashed curves. By plotting the natural logarithm of G/G_i versus layer thickness as in Fig. 6, these curves appear almost identical to the corresponding ones in Fig. 5. The sheet conductance decreases sharply at the thicknesses where the barrier height also does. This can be expected from the expression, Eq. (11), and suggests the sheet conductance as a direct experimental measurement of the barrier height.

The above features illustrated by Figs. 4—6 are also seen with a finite thickness of i-type layers interposed between p- and n-type layers. Replacing a part of the doped layer with the i-type layer leads to the decay of barrier height to start at a larger thickness (S) as shown in Fig. 7.

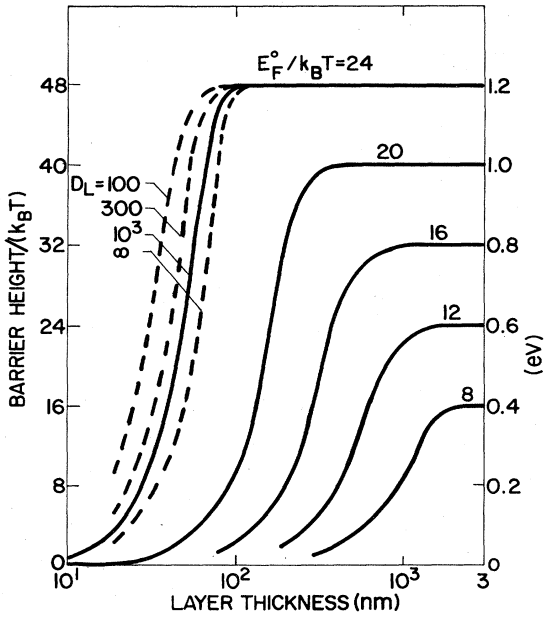

FIG. 5. Barrier height as a function of layer thickness calculated for antisymmetric n-p multilayers of various Fermi energies E_F^0. The Debye lengths are $D_i = 10^6$ nm for all curves, and $D_L = 10^3$ nm for the solid curves. The D_L values for the dashed curves are marked in the figure (in nm).

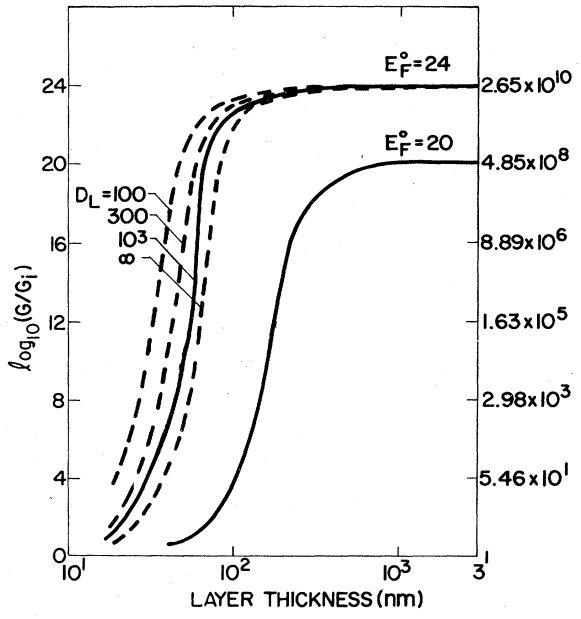

FIG. 6. Sheet conductance G, normalized to $G_i = q\mu n_i S/2$, as a function of layer thickness, calculated from the same potential distributions used to generate Fig. 5 ($E_F^0 = 20 k_B T$ and $24 k_B T$ only).

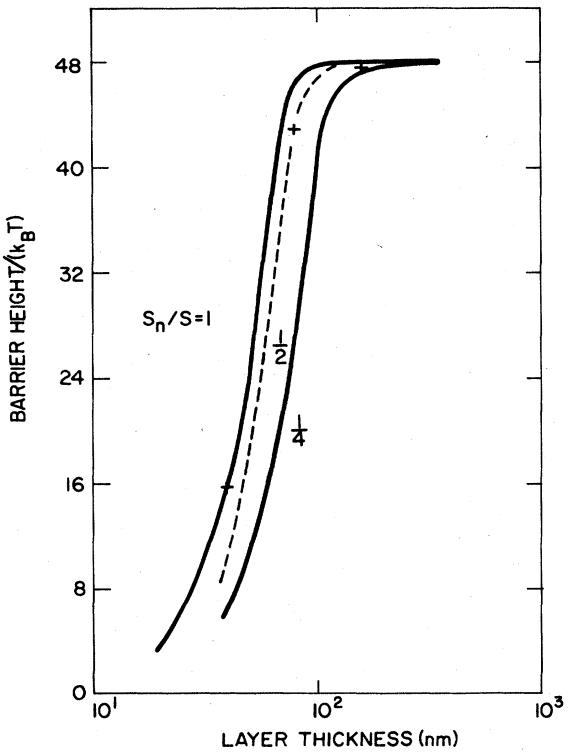

FIG. 7. Barrier height vs layer thickness calculated for antisymmetric n-i-p-i multilayers of Fermi energies $E_F^0=\pm 24k_BT$. The ratios of doped-layer thickness to half-period are $S_n/S=1$, $\frac{1}{2}$, and $\frac{1}{4}$. The three crosses denote the data for a fixed S_n ($=40$ nm) with different i-type layer thicknesses of 0, 40, and 120 nm, respectively.

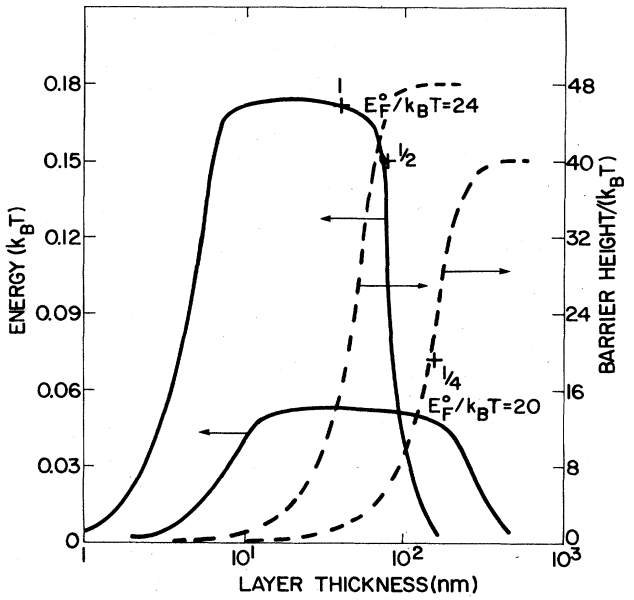

FIG. 8. First-order quantized energy in an antisymmetric n-p multilayer of Fermi energies $E_F^0=\pm 20k_BT$ and $\pm 24k_BT$, as a function of layer thickness. The potential distributions used are the same as those of solid curves in Fig. 5. The barrier height (dashed curve) is reproduced from Fig. 5 for comparison. The three crosses are data for n-i-p-i multilayers corresponding to the three data on Fig. 7.

The thicknesses of the doped layer are 100%, 50%, and 25% of the half-period S, respectively, for the three curves. On the other hand, for a given thin doped layer, the barrier height can be increased (up to $2E_F^0$) by interposing an i-type layer. This is illustrated by the three data points (+) in Fig. 7. In these cases the doped layer thicknesses are the same (40 nm), but the i-type layer thicknesses are 0, 40, and 120 nm, respectively. However, this increased barrier height does not mean an enhancement of the quantum well effect by the i-type layer, because the period of the superlattice has also increased. This can be seen quantitatively from the calculations of the quantized energy levels presented below.

B. Quantized energies and wave functions

The quantized energy levels calculated by the method of Sec. II B (assuming $m^*=$ rest mass) and using the potentials obtained above for n-p multilayers are shown as a function of the layer thickness in Fig. 8 for $E_F^0=20k_BT$ and $24k_BT$. The corresponding barrier heights (dashed curves) are reproduced from Fig. 5 for comparison. It can be seen that the quantized energy level increases with decreasing layer thickness, in spite of the lowering of barrier height, to a maximum value of $\approx 0.05k_BT$ and $\approx 0.17k_BT$, for $E_F^0=20k_BT$ and $24k_BT$, respectively, at layer thicknesses of several tens of nm. Further decrease in the layer thickness cannot increase the energy because of the diminishing barrier height. The three data points (+) are the calculated energies for the three cases with the same doped layer thickness (40 nm) but different i-type layer thicknesses, cf. Fig. 7.

Persistent photoconductivity (PPC) has been observed[7] in a-Si:H n-p superlattices of layer thickness $S=27$ to 50 nm. While this thickness is an order of magnitude larger than that of a-Si:H compositional superlattices reported in the literature,[2–6] it is consistent with the findings from the present theoretical studies. The calculations above have indicated that at smaller thicknesses than this, the space charge doping effect would diminish the barrier which makes PPC possible. It can be predicted that a thickness dependence study of PPC will find the optimum thickness in this range of layer thickness.

Even with the high doping levels assumed in this example, the quantized energy is only a small fraction of $1k_BT$. Although it is still larger than that expected from a square-well potential,[12] it is much smaller than the energy fluctuation due to the effects of disorder in amorphous semiconductors. Therefore, while it is consistent with the persistent photoconductivity data, the concept of quantum-well effect in amorphous semiconductor multilayers should be taken cautiously.

IV. SUMMARY AND CONCLUSION

The effects of space-charge doping in n-i-p-i doping superlattices (in particular, of a-Si:H) are quantitatively analyzed. First, the electronic potential distribution in the

multilayer is calculated by solving Poisson's equation. Then, the quantized energy and wave function of an electron in this potential are determined by numerical solution of the Schrödinger equation. It is demonstrated that space-charge doping decreases the barrier height significantly as the layer thickness is reduced. Therefore, it acts as a counter doping, and the layer behaves more intrinsic-like than its constituent semiconductors. This accounts for the observed blue shift of the photoluminescence peak.[7] Another consequence of the reduction of barrier height with thickness is the existence of an optimum thickness for carrier confinement in the layer. In *a*-Si:H, it is found to be in the range of several tens of nm. This is nearly an order of magnitude larger than the thickness of *a*-Si:H compositional superlattices in which the quantum effects are found, experimentally[2–6] and theoretically,[8] to be most significant. Yet, this is the thickness of *a*-Si:H doping superlattices in which persistent photoconductivity has been observed.[7] This distinction between the critical thicknesses in the two types of superlattices arises from the significant barrier height reduction due to space-charge doping in doping superlattices. This is quantitatively elucidated by the analyses in this and the following paper.[8]

---

[1]K. Ploog and G. H. Dohler, Adv. Phys. **32**, 285 (1983).
[2]H. Munekata, M. Mizuta, and H. Kukimoto, J. Non-Cryst. Solids **59-60**, 1167 (1983); Jpn. J. Appl. Phys. **22**, L544 (1983).
[3]M. Hirose and S. Miyazaki, J. Non-Cryst. Solids **66**, 327 (1984).
[4]J. Kakalios, H. Fritzsche, N. Ibaraki, and S. R. Ovshinsky, J. Non-Cryst. Solids **66**, 339 (1984).
[5]T. Tiedje, B. Abeles, P. D. Persans, B. G. Brooks, G. D. Cody, J. Non-Cryst. Solids **66**, 345 (1984); **66**, 351 (1984); B. Abeles and T. Tiedje, Phys. Rev. Lett. **51**, 2003 (1983).
[6]C. B. Roxlo, B. Abeles, and T. Tiedje, Phys. Rev. Lett. **52**, 1994 (1984).
[7]J. Kakalios and H. Fritzsche, Phys. Rev. Lett. **53**, 1602 (1984).
[8]I. Chen, following paper, Phys. Rev. B **32**, 885 (1985).
[9]The derivation of Eq. (6) can be found in Refs. 10 and 11. Since the functional forms of the localized-state distributions are not known exactly, the use of mathematically simpler "zero-temperature" statistics is appropriate. It does not imply that the formula is strictly applicable only at $T=0$. The result using finite-temperature Fermi statistics (see Ref. 10) differs from Eq. (6) in a constant factor of order unity.
[10]I. Chen and S. Lee, J. Appl. Phys. **53**, 1045 (1982).
[11]I. Chen, J. Appl. Phys. **56**, 396 (1984).
[12]C. Kittel, *Introduction to Solid State Physics*, 5th ed. (Wiley, New York, 1976).
[13]W. E. Spear, Adv. Phys. **26**, 811 (1977).
[14]R. A. Street, D. K. Biegelsen, and J. C. Knights, Phys. Rev. B **24**, 969 (1981).